

# Journal of Biomedical Optics

[SPIEDigitalLibrary.org/jbo](http://SPIEDigitalLibrary.org/jbo)

## **Functional probe for annulus fibrosus-targeted intervertebral disc degeneration imaging**

Hye-Yeong Kim  
Michael McClincy  
Nam V. Vo  
Gwendolyn A. Sowa  
James D. Kang  
Mingfeng Bai

# Functional probe for annulus fibrosus-targeted intervertebral disc degeneration imaging

Hye-Yeong Kim,<sup>a\*</sup> Michael McClincy,<sup>b\*</sup> Nam V. Vo,<sup>b</sup> Gwendolyn A. Sowa,<sup>b,c</sup> James D. Kang,<sup>b</sup> and Mingfeng Bai<sup>a,d</sup>

<sup>a</sup>University of Pittsburgh, Department of Radiology, School of Medicine, Molecular Imaging Laboratory, Pittsburgh, Pennsylvania 15219

<sup>b</sup>University of Pittsburgh Medical Center, Department of Orthopedic Surgery, Ferguson Laboratory for Orthopaedic Research, Pittsburgh, Pennsylvania 15213

<sup>c</sup>University of Pittsburgh Medical Center, Department of Physical Medicine and Rehabilitation, Pittsburgh, Pennsylvania 15213

<sup>d</sup>University of Pittsburgh Cancer Institute, Pittsburgh, Pennsylvania 15213

**Abstract.** Intervertebral disc degeneration (IDD) is closely associated with low back pain. Typically nonsurgical treatment of IDD is the most effective when detected early. As such, establishing reliable imaging methods for the early diagnosis of disc degeneration is critical. The cellular and tissue localization of a facile functional fluorescent probe, HYK52, that labels disc annulus fibrosus is reported. HYK52 was synthesized with high yield and purity via a two-step chemical reaction. Rabbit disc cell studies and *ex vivo* tissue staining images indicated intracellular localization and intervertebral disc (IVD) tissue binding of HYK52 with negligible cytotoxicity. Moreover, HYK52 is purposefully designed with a functional terminal carboxyl group to allow for coupling with various signaling molecules for multimodal imaging applications. These results suggest that this IVD-targeted probe may have great potential in early diagnosis of IDD. © 2013 Society of Photo-Optical Instrumentation Engineers (SPIE) [DOI: 10.1117/1.JBO.18.10.101308]

Keywords: fluorescence imaging; intervertebral disc degeneration; imaging probe; annulus fibrosus; early diagnosis.

Paper 130112SSR received Feb. 28, 2013; revised manuscript received May 9, 2013; accepted for publication Jun. 3, 2013; published online Jul. 9, 2013.

## 1 Introduction

Low back pain (LBP) is the primary cause of activity limitation in patients below the age of 45. Upward of 80% of the U.S. population will be effected by LBP at some point in their lifetime.<sup>1</sup> Although LBP is a complicated condition with many possible etiologies, intervertebral disc degeneration (IDD) is believed to play a significant role (40% to 50% of all cases) in the development of this condition.<sup>2</sup> The intervertebral disc (IVD) consists of a fibrocartilaginous ring called the annulus fibrosus (AF), which surrounds the proteoglycan-rich nucleus pulposus (NP). Both structures are heavily imbibed with water, providing hydrostatic pressure to serve as a “shock absorber” of axial loads. IDD is thought to be a result of a combination of aging, abnormal mechanical stress, genetic predisposition, and environmental factors such as tobacco smoking. The common outcome of IDD is imbalanced disc matrix homeostasis leading to the net loss of extracellular matrix structure and water content.<sup>3–5</sup> Despite its prevalence, IDD has proven to be a difficult disease process to treat as the disc is a highly avascular structure with little inherent ability for repair or regeneration.<sup>6</sup> Current areas of research focusing on treatment include physical therapy, spinal injections, molecular and gene therapy, stem cell therapy, and surgeries.<sup>7–10</sup> A unifying consensus of these treatment modalities is that early identification of disc tissue damage will aid in the treatment and recovery process.

For diagnosis of IDD via spine morphology imaging, several noninvasive imaging modalities are currently available, including computed tomography and magnetic resonance imaging

(MRI).<sup>11–13</sup> As disc degeneration primarily involves changes in soft tissue structure, MRI has been a well-studied method for the evaluation of IDD.<sup>14–17</sup> Standard MR sequences such as T1 and T2 have significant limitations in detecting early IDD changes,<sup>14–17</sup> and commonly used MR contrast agents such as gadolinium (Gd) have also been shown to have limited clinical utility due to poor target specificity and low penetration efficiency within the disc.<sup>18,19</sup> The goal of this article was to develop and evaluate a novel fluorescent probe that specifically targets AF, the tissue that forms the outer layer of the disc. Fluorescence imaging is a relatively low-cost imaging method with high sensitivity and resolution. In addition, we incorporated a functional terminal carboxyl group in the probe design to allow for coupling with various signaling molecules for multimodal imaging applications. Fusing fluorescence imaging with other imaging modalities will combine the advantages of each imaging modality to improve diagnostic accuracy and better characterize the disease processes.<sup>20</sup> This will also allow translational imaging of IDD from the molecular level to clinical scales. Through imaging AF with a targeted probe, we will have the opportunity to visualize the molecular, cellular, and morphological changes that are associated with the early stage of IDD.

A recent study by Gibbs-Strauss et al. described the AF tissue-specific uptake of the fluorescent styryl pyridinium (FM) dyes in IVD.<sup>21</sup> However the utility of these FM molecules is limited in IDD imaging due to the penetration limitation of the fluorescent signal, especially in the visible region, where FM dyes emit. Moreover, the lack of functional group on these FM molecules prevents them from being imaged by other imaging techniques. In this study, we developed a functional fluorescent IVD-targeted probe, HYK52, with a terminal

\*Hye-Yeong Kim and Michael McClincy equally contributed.

Address all correspondence to: Mingfeng Bai, University of Pittsburgh School of Medicine, Department of Radiology, Molecular Imaging Laboratory, 100 Technology Drive Suite 452G, Pittsburgh, Pennsylvania 15219. Tel: +1-412-624-2565; Fax: +1-412-624-2598; E-mail: [baim@upmc.edu](mailto:baim@upmc.edu)

carboxyl group that has the potential to couple with a wide range of signaling moieties, such as chelated radioisotopes (for positron emission tomography) and  $Gd^{3+}$  (for MRI). Multimodal imaging approach will address the penetration issue of fluorescence imaging in the visible region by introducing an additional imaging modality that has no penetration limitation. It also improves diagnostic accuracy and better characterizes disease processes through combining the advantages of each imaging modality. Therefore, such a tunable probe will have great potential in studying disc morphology by providing disc-targeted image contrast through noninvasive means.

## 2 Methods and Materials

Unless otherwise stated, all chemical reagents were purchased from commercial sources and used without further purifications. Gadobenate dimeglumine (Gd-BOPTA, Multihance, Bracco Diagnostics Inc., Princeton, New Jersey) was obtained from the vendor. Silica gel (240 to 400 mesh, Sorbtech) was used for column chromatography. NMR spectra were obtained from Bruker 400 MHz, and deuterated solvents were purchased from Cambridge Laboratory (Andover, Massachusetts). Mass spectrometry was performed using electrospray ionization mass spectrometry (ESI/MS; Waters 2998 photodiode array detector).

### 2.1 Spectroscopy

Absorbance of compounds was measured using a Cary 100 Bio UV/Visible spectrophotometer. Fluorescence spectra were collected on a Cary Eclipse fluorescence spectrophotometer. Optical properties of compounds were measured using quartz fluorometer cuvettes (Starna Cells Inc., Atascadero, CA) at room temperature. Fluorescence images of fixed cells were recorded with the Zeiss Axiovert 40 calibrated focal length (CFL) fluorescence microscope using a red fluorescent protein (RFP) filter. Cryosectioned tissue images were captured with DP2-BSW software (Olympus, Center Valley, Pennsylvania) using a Nikon TE-2000U Eclipse microscope equipped with a DP71 camera (Olympus, Center Valley, Pennsylvania).

### 2.2 Synthesis of HYK52

1-(2-Carboxyethyl)-4-methylpyridin-1-ium bromide, compound 1, was synthesized according to a known procedure.<sup>22,23</sup> To a solution of compound 1 (1 g, 4.08 mmol) in ethanol (7 mL), piperidine (2.02 mL, 20.4 mmol) was added. *N* - *N'*-dibutylaminobenzaldehyde (0.99 mL, 4.08 mmol) was added drop wise, and the reaction mixture was heated at 60°C to 70°C overnight to form a dark red precipitate. After the solvent was removed by rotary evaporation, the crude was purified by silica gel column chromatography dichloromethane (DCM: MeOH = 1/5). The reddish powder was obtained in 97% yield. <sup>1</sup>H NMR (MeOD-d<sub>4</sub>, 400 MHz)  $\delta$ 8.45 (d, 2H, *J* = 6.9 Hz), 7.76 (d, 2H, *J* = 7.0 Hz), 7.65 (d, 1H, *J* = 16 Hz), 7.45 (d, 2H, *J* = 9.0 Hz), 6.9 (d, 1H, *J* = 16 Hz), 6.60 (d, 2H, *J* = 9.04 Hz), 4.49 (t, 2H, *J* = 6.28 Hz, 6.32 Hz), 3.29 (t, 4H, *J* = 7.56 Hz, 7.80 Hz), 3.21 (q, 2H, *J* = 1.64 Hz), 2.69 (t, 2H, *J* = 6.32 Hz, 6.28 Hz), 1.50 (m, 4H), 1.29 (M, 4H), 0.88 (t, 6H, *J* = 7.32 Hz, 7.40 Hz), <sup>13</sup>C NMR (MeOD-d<sub>4</sub>, 100 MHz) 176.5, 156.2, 151.9, 144.6, 144.2, 131.9, 123.4, 123.2, 117.2, 112.8, 58.6, 54.8, 51.7, 49.8, 39.5, 30.6, 21.2, 14.3 M/S(ESI): calculated for C<sub>24</sub>H<sub>33</sub>N<sub>2</sub>O<sub>2</sub><sup>+</sup> [M]<sup>+</sup> m/z 381.25, found m/z 381.17 [M]<sup>+</sup>.

### 2.3 Isolation and Cell Culture of Annulus Fibrosus and Nucleus Pulposus

IVDs from skeletally mature New Zealand white rabbits were dissected immediately after sacrifice. Under sterile conditions, the AF and NP were separated and minced, washed with Hanks balanced salt solution, and digested in culture media containing 5% fetal bovine serum (FBS), 1% penicillin-streptomycin (P/S), and 0.2% pronase for 60 min. Medium was changed to different media solution containing 5% FBS, 1% P/S, 0.02% Collagenase-P and incubated for 18 h. Released cells were centrifuged for 5 min at 2000 rpm, counted, and plated into standard tissue culture flasks incubated at 37°C under 5% CO<sub>2</sub> until the cells reached ~90% confluency.

### 2.4 Cytotoxicity (XTT) Assay

Ninety-six-well plates were inoculated with 2500 cells per well with either AF or NP cell types. The cells were incubated in F12 media with 1% P/S and 10% FBS (standard media) for 72 h to allow cellular adherence to the plate. After 72 h, culture media were changed to the experimental conditions: no treatment, 1 mM NaOH, 50 and 100  $\mu$ g/mL (108 and 217  $\mu$ M) HYK52, and 50 and 100  $\mu$ g/mL (75 and 150  $\mu$ M) gadolinium (Gd-BOPTA) in cell culture media. Gadolinium (Gd-BOPTA) was included in the cytotoxicity 2,3-Bis-(2-methoxy-4-nitro-5-sulphophenyl)-2H-tetrazolium-5-carboxanilide disodium salt (XTT) assay as it is the modern standard for intravenous contrast in MRI. The conditions of 50 and 100  $\mu$ g were chosen as the peak plasma concentration of gadolinium after a standard intravenous dose was calculated at 100  $\mu$ g/mL, calculated from standard weight-based dosing protocols and average circulating blood volume. Thus, peak and half-strength doses were observed in the cytotoxicity assay. The cells were exposed to the experimental conditions for 24, 48, and 72 h. After appropriate exposure, the experimental medium was removed and the cells were washed three times with sterile phosphate-buffered saline (PBS). After washing, 100  $\mu$ L of F12 1% P/S media without FBS was added to each well. Cells were then exposed to 50  $\mu$ L of a 99% XTT/1% phenazine methosulphate (PMS) solution (Sigma) and incubated for 4 h. Following incubation, light absorption at 690 nm was measured. This process was repeated three times for each cell type with different cell lines. XTT assay results reflect the presence of mitochondrial enzyme activity within a cell culture, requiring metabolically active cells for formazan dye reduction. Thus, while the assay does not directly measure cellular viability, the measurement of metabolic activity accurately reflects overall cellular survival. Simple *t* tests were conducted to identify statistically significant differences in cytotoxicity at each time point.

### 2.5 Disc Cellular Uptake Study

Twenty-four well plates were inoculated with 20,000 cells per well for both AF and NP cells. The cells were incubated in standard media for 72 h to allow cellular adherence. After the 72-h period of cell adhesion, cells were treated with 122  $\mu$ M HYK52 in culture media for 24 h. Following this incubation, cells were washed three times with sterile PBS and then fixed with paraformaldehyde (PFA) for 15 min at room temperature. After fixation, PFA was removed and cells were washed with PBS three times. All images were captured in bright field and fluorescence

with the Zeiss Axiovert 40 CFL fluorescence microscope using an RFP filter (excitation: 545 nm; emission: 620 nm).

## 2.6 Ex Vivo Disc Tissue Staining

Whole spine specimens from skeletally mature New Zealand white rabbits were dissected immediately after sacrifice. The posterior vertebral structures and spinal cord were removed, and the cartilaginous zones (endplates and epiphyses) were dissected from the vertebral bodies on both sides of the disc. These disc units were then incubated in culture media containing 122  $\mu\text{M}$  HYK52 for 24 h, washed three times with sterile PBS, and then incubated again for 2 h in standard media. Following this incubation, disc was mounted in TissueTek optimal cutting temperature compound (Fischer-Scientific, Hampton, New Hampshire), flash-frozen in liquid nitrogen, and stored in a  $-80^\circ\text{C}$  freezer. Each sample was cryosectioned to a thickness of 10  $\mu\text{m}$  per slice. All images were captured with DP2-BSW software (Olympus) using a Nikon TE-2000U Eclipse microscope at 2 $\times$  magnification with an RFP filter set equipped with a DP71 camera (Olympus).

## 3 Results and Discussion

Figure 1 shows the synthetic pathway of HYK52. The pyridinium salt, compound 1, was synthesized by a known procedure.<sup>22,23</sup> An aldol condensation reaction with *N*-*N'*-dibutylaminobenzaldehyde in the presence of piperidine yielded HYK52 as a dark red powder with >95% yield. The structures of synthesized compounds were characterized by NMR and ESI/MS. The maximum absorption and emission of HYK52 occur at 490 and 613 nm ( $\lambda_{\text{ext}} = 495$  nm in methanol), respectively, with extinction coefficient ( $\epsilon$ ) of 12,863  $\text{M}^{-1} \text{cm}^{-1}$  (Fig. 2). In water, the absorption and emission peaks were blue-shifted by roughly

10 nm, and the extinction coefficient decreased 2.4-fold ( $\epsilon = 5360 \text{ M}^{-1} \text{cm}^{-1}$ ).

To test whether HYK52 has cytotoxic effects on disc cells, AF and NP cells were exposed to synthesized HYK52 and cell viability was measured using the XTT assay. Disc cells isolated from New Zealand white rabbits were incubated with two concentrations of HYK52 (50 and 100  $\mu\text{g}/\text{mL}$  or 108 and 217  $\mu\text{M}$ ) for 24 h (Fig. 3). Gadolinium (Gd-BOPTA) was included in the cytotoxicity assay as it is the modern standard for intravenous contrast in MRI. The concentrations of 50 and 100  $\mu\text{g}/\text{mL}$  (75 and 150  $\mu\text{M}$ ) were chosen because the peak plasma concentration of Gd-BOPTA after a standard intravenous dose was calculated at 100  $\mu\text{g}/\text{mL}$  from standard weight-based dosing protocols and average circulating blood volume. Thus, peak (100  $\mu\text{g}/\text{mL}$ ) and half-strength (50  $\mu\text{g}/\text{mL}$ ) doses were used in the cytotoxicity assay. Cells treated with 1 mM NaOH solution to induce complete cell death were included as a positive control. Compared to both untreated cells and clinically approved Gd-BOPTA, HYK52 showed no significant cell cytotoxicity at the experimental concentrations. Similar results were observed for cells exposed for 48 and 72 h (data not shown). As expected, cells treated with NaOH showed a significantly higher rate of cytotoxicity in both AF and NP cells at all time points.

Disc cells were incubated with the fluorescent HYK52 to evaluate cellular uptake. Time- and concentration-dependent cellular localizations were studied in both AF and NP cells (Figs. 4 and 5). Greater fluorescence was seen in AF cells compared to NP cells after 24 h of incubation, suggesting more efficient HYK52 uptake by AF cells (Fig. 4). After 48 h, NP disc cells also showed significant fluorescence signal. Cells treated with the higher concentration of HYK52 (122  $\mu\text{M}$ , 56  $\mu\text{g}/\text{mL}$ ) showed more intense fluorescence signal than those treated with the lower concentration (61  $\mu\text{M}$ , 28  $\mu\text{g}/\text{mL}$ ) (Fig. 5). The small

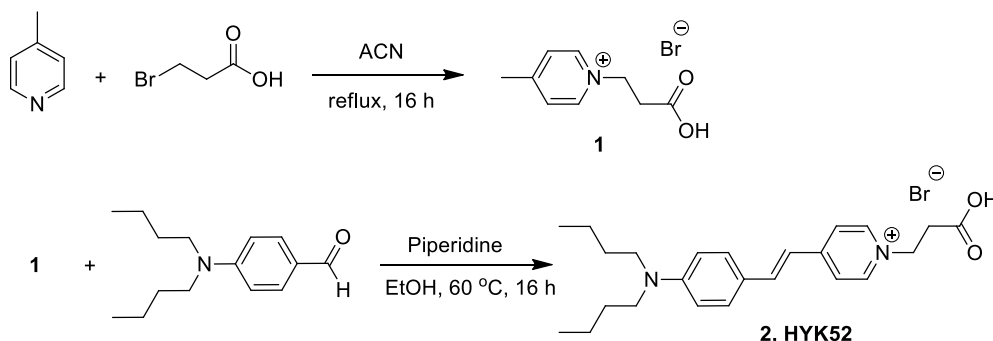


Fig. 1 Synthesis of functional AF-targeted probe, HYK52.

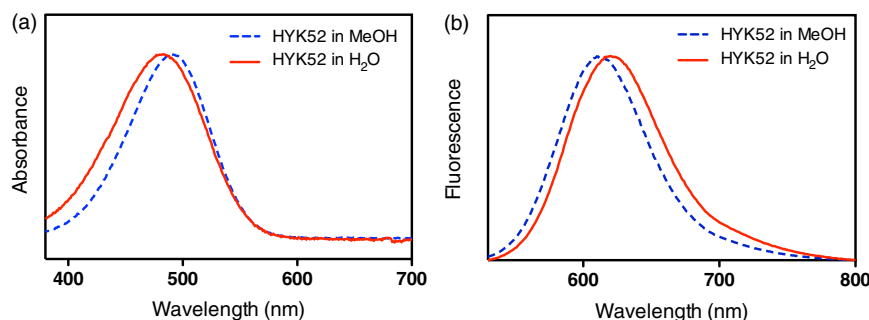
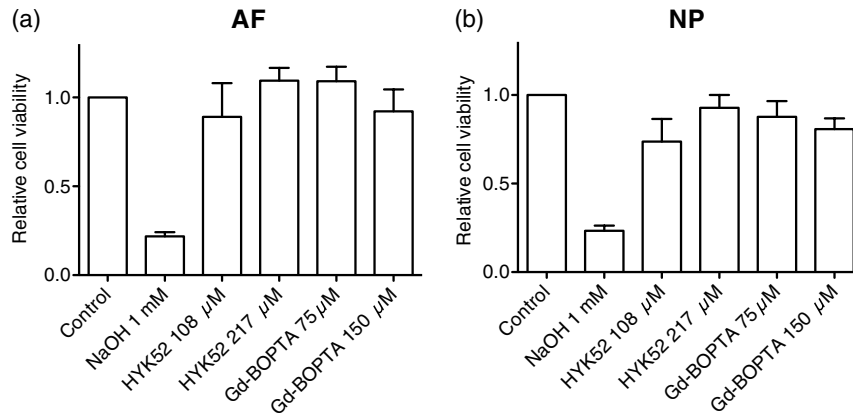
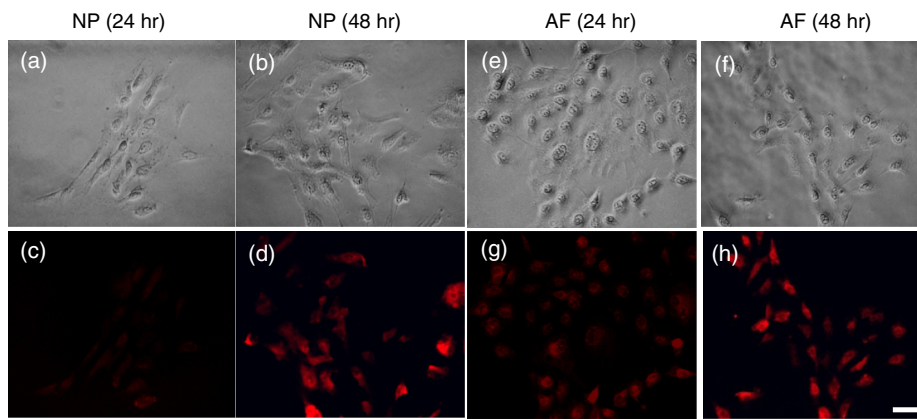


Fig. 2 Absorption (a) and emission (b) spectra of HYK52 in methanol (blue) and water (red) ( $\lambda_{\text{ext}} = 495$  nm).



**Fig. 3** HYK52 has minimal cytotoxicity on disc cells. Annulus fibrosus (AF) (a) and nucleus pulposus (NP) (b) cells were incubated with 0, 108, and 217 μM HYK52 for 24 h and cell viability was measured using the XTT assay. Clinically approved gadobenate dimeglumine (Gd-BOPTA) was used for comparison. Error bars represent s.d. from triplicates.



**Fig. 4** Time-dependent HYK52 cellular uptake. NP [(a), (b), (c), and (d)] and AF [(e), (f), (g), and (h)] cells were incubated with 122 μM HYK52 for 24 and 48 h. Bright field [(a), (b), (e), and (f)] and fluorescence [(c), (d), (g), and (h)] images were taken after fixation. Scale bar, 20 μm (magnification ×400).

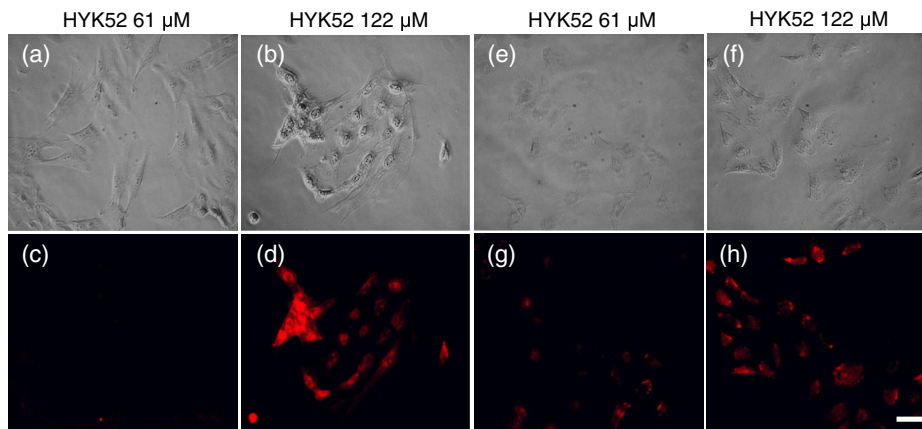


**Fig. 5** Concentration-dependent HYK52 cellular uptake. NP [(a), (b), (c), and (d)] and AF [(e), (f), (g), and (h)] cells were incubated with 61 and 122 μM HYK52 for 48 h. Bright field [(a), (b), (e), and (f)] and fluorescence [(c), (d), (g), and (h)] images were taken after fixation. Scale bar, 20 μm (magnification ×400).

lipophilic HYK52 dye was localized primarily to the cytosol of both AF and NP cells. It is possible that HYK52 was internalized through passive diffusion; however, elucidation of the exact mechanism is beyond the scope of this study.

Rabbit IVDs soaked in HYK52 showed strong fluorescence signals in the AF region of the IVD (Fig. 6). Three different incubation time periods, including 24, 48, and 72 h, were

used for this study and the imaging results were similar. The data from 24-h incubation time were selected (Fig. 6). HYK52 binding in the AF highlighted the lamellar striations of the fibrocartilage structure, and stronger fluorescence was observed toward the disc's periphery than at the inner annulus. The relatively weak fluorescence pattern observed in the NP region accurately reflects its less organized structure.

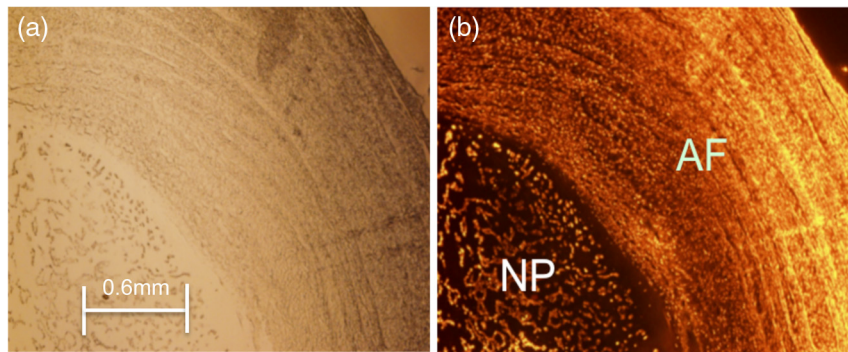


**Fig. 6** Rabbit disc tissue microscopy images. The dissected rabbit discs were soaked in media containing HYK52 (122  $\mu$ M) and incubated for 24 h. After washing and fixation, frozen tissue was cryosectioned in 10  $\mu$ m thickness for imaging. Bright field (a) and fluorescence (b) images at 2 $\times$  magnification.

#### 4 Summary

In summary, HYK52 was synthesized with high yield and purity via a two-step chemical reaction. Cell viability test indicated negligible cytotoxicity of HYK52 in tested concentrations compared to the clinically approved MRI contrast agent, Gd-BOPTA. Disc cells readily uptake HYK52, with AF cells appearing to be more efficient than NP cells in this process. This is evident by the higher fluorescence signal in AF cells compared to that in NP cells after 24 h of incubation. Fluorescence imaging of rabbit disc specimen demonstrated the high localization of HYK52, which highlighted the lamellar striations of the fibrocartilage structure. These results indicate that HYK52 is biocompatible and has great potential in IVD-targeted imaging. Although HYK52 is not suitable for *in vivo* imaging due to the unfavorable emission wavelength in the visible region, introduction of additional imaging moieties that do not have penetration limitation can be readily achieved through bioconjugation with the carboxyl group on HYK52. Synthesis and *in vivo* imaging of HYK52-based multimodal imaging probes is currently ongoing.

#### Acknowledgments

We thank Dr. Michael Modo, Dr. Chan-hong Moon, and Lloydine Jacobs at the University of Pittsburgh for providing technical advices and support to this work. This work was supported by the startup fund provided by the Department of Radiology, University of Pittsburgh (Mingfeng Bai), and National Institutes of Health grant AG033046 (Nam Vo).

#### References

- G. B. Andersson, "Epidemiology of low back pain," *Acta orthopaedica Scandinavica. Supplementum* **281**, 28–31 (1998).
- American Academy of Orthopaedic Surgeons et al., "Spine: low back and neck pain," in *The Burden of Musculoskeletal Diseases in the United States*, J. J. Jacobs, Ed., pp. 21–56, Bone and Joint Initiative, Rosemont, Illinois (2011).
- P. Goupille, D. Mulleman, and X. Chevalier, "Is interleukin-1 a good target for therapeutic intervention in intervertebral disc degeneration: lessons from the osteoarthritic experience," *Arthritis Res. Ther.* **9**(6), 110–111 (2007).
- C. L. LeMaitre et al., "Matrix synthesis and degradation in human intervertebral disc degeneration," *Biochem. Soc. Trans.* **35**(Pt 4), 652–655 (2007).
- K. Yong-Hing and W. H. Kirkaldy-Willis, "The pathophysiology of degenerative disease of the lumbar spine," *Orthop. Clin. North Am.* **14**(3), 491–504 (1983).
- J. P. Urban, S. Smith, and J. C. Fairbank, "Nutrition of the intervertebral disc," *Spine (Phila Pa 1976)* **29**(23), 2700–2709 (2004).
- K. Masuda and H. S. An, "Prevention of disc degeneration with growth factors," *Eur. Spine J.* **15**(Suppl. 3), S422–S432 (2006).
- S. H. Moon et al., "Human intervertebral disc cells are genetically modifiable by adenovirus-mediated gene transfer: implications for the clinical management of intervertebral disc disorders," *Spine (Phila Pa 1976)* **25**(20), 2573–2579 (2000).
- F. H. Shen, D. Samartzis, and G. B. Andersson, "Nonsurgical management of acute and chronic low back pain," *J. Am. Acad. Orthop. Surg.* **14**(8), 477–487 (2006).
- F. Yang et al., "Mesenchymal stem cells arrest intervertebral disc degeneration through chondrocytic differentiation and stimulation of endogenous cells," *Mol. Ther.* **17**(11), 1959–1966 (2009).
- D. Butler et al., "Discs degenerate before facets," *Spine (Phila Pa 1976)* **15**(2), 111–113 (1990).
- B. L. Sachs et al., "Dallas discogram description. a new classification of CT/discography in low-back disorders," *Spine (Phila Pa 1976)* **12**(3), 287–294 (1987).
- K. D. M. Stumpe et al., "FDG positron emission tomography for differentiation of degenerative and infectious endplate abnormalities in the lumbar spine detected on MR imaging," *Am. J. Roentgenol.* **179**(5), 1151–1157 (2002).
- L. M. Benneker et al., "Correlation of radiographic and MRI parameters to morphological and biochemical assessment of intervertebral disc degeneration," *Eur. Spine J.* **14**(1), 27–35 (2005).
- R. Gunzburg et al., "A cadaveric study comparing discography, magnetic resonance imaging, histology, and mechanical behavior of the human lumbar disc," *Spine (Phila Pa 1976)* **17**(4), 417–426 (1992).
- C. W. Pfirrmann et al., "Effect of aging and degeneration on disc volume and shape: a quantitative study in asymptomatic volunteers," *J. Orthop. Res.* **24**(5), 1086–1094 (2006).
- M. L. Schiebler et al., "In vivo and ex vivo magnetic resonance imaging evaluation of early disc degeneration with histopathologic correlation," *Spine (Phila Pa 1976)* **16**(6), 635–640 (1991).
- R. K. Breger et al., "Contrast enhancement in spinal MR imaging," *Am. J. Roentgenol.* **153**(2), 387–391 (1989).
- G. Akansel et al., "Diffusion into human intervertebral disks studied with MR and gadoteridol," *Am. J. Neuroradiol.* **18**(3), 443–445 (1997).
- D. Majumdar, X. H. Peng, and D. M. Shin, "The medicinal chemistry of theragnostics, multimodality imaging and applications of nanotechnology in cancer," *Curr. Top. Med. Chem.* **10**(12), 1211–1226 (2010).
- S. L. Gibbs-Strauss et al., "Molecular imaging agents specific for the annulus fibrosus of the intervertebral disk," *Mol. Imag.* **9**(3), 128–140 (2010).
- A. Hassner, D. Birnbaum, and L. M. Loew, "Charge-shift probes of membrane potential. Synthesis," *J. Org. Chem.* **49**(14), 2546–2551 (1984).
- R. Krieg et al., "Optimization of heterocyclic 4-hydroxystyryl derivatives for histological localization of endogenous and immunobound peroxidase activity," *Biotech. Histochem.* **82**(4–5), 235–262 (2007).